Wei Han, Mei Li, Xiang Geng and Guoshun Zhang*

The cocrystal structure of praziquantel-hesperetin (1/1), $C_{35}H_{38}N_2O_8$

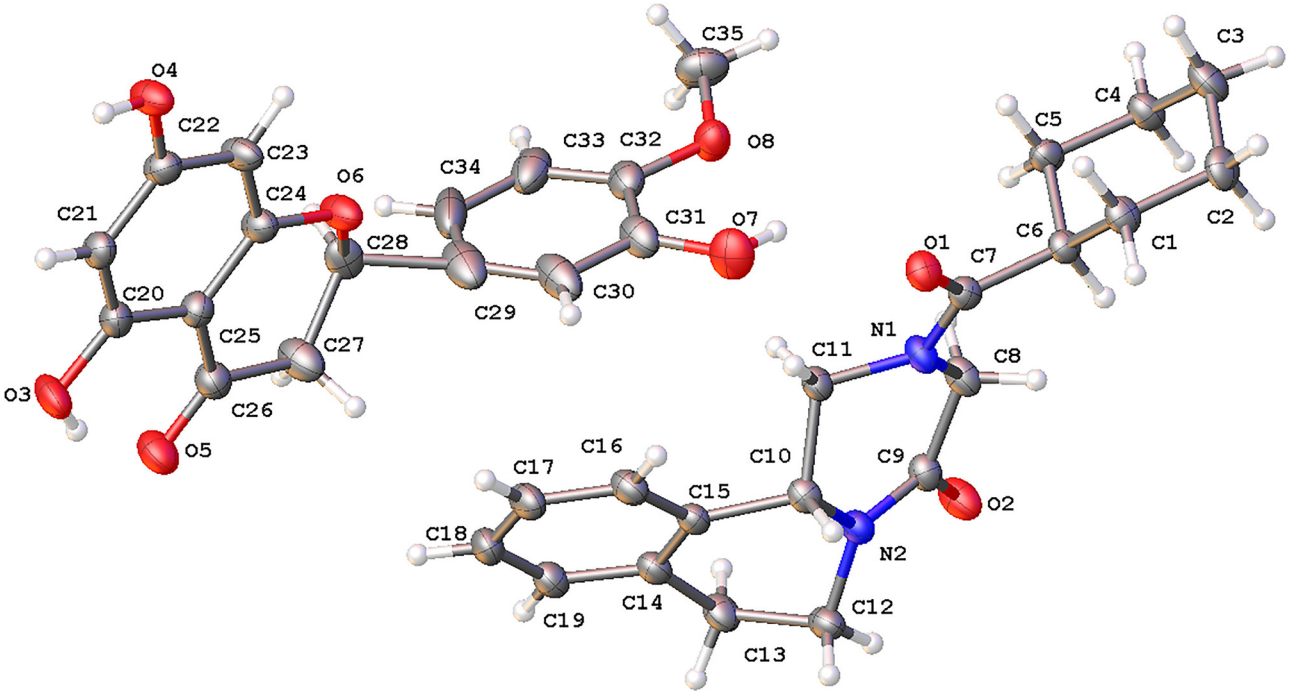

https://doi.org/10.1515/ncrs-2024-0340
Received August 14, 2024; accepted October 18, 2024;
published online November 26, 2024

Abstract

$C_{35}H_{38}N_2O_8$, monoclinic, $P2_1$ (no. 4), a = 14.0502(3) Å, b = 5.93007(14) Å, c = 18.3417(4) Å, β = 101.327(2)°, V = 1498.45(6) Å^3, Z = 2, $R_{gt}(F)$ = 0.0443, w$R_{ref}(F^2)$ = 0.1082, T = 100(2) K.

CCDC no.: 2377413

The molecular structure is shown in the figure. Table 1 contains crystallographic data and Table 2 contains the list of the atoms including atomic coordinates and displacement parameters.

Table 1: Data collection and handling.

Crystal:	Colourless block
Size:	0.30 × 0.20 × 0.20 mm
Wavelength:	Cu *K*α radiation (1.54184 Å)
μ:	0.79 mm^{-1}
Diffractometer, scan mode:	ROD, Synergy Custom DW system, HyPix, ω
θ_{max}, completeness:	75.9°, 99 %
$N(hkl)_{measured}$, $N(hkl)_{unique}$, R_{int}:	17393, 5940, 0.028
Criterion for I_{obs}, $N(hkl)_{gt}$:	$I_{obs} > 2\sigma(I_{obs})$, 5809
N(param)$_{refined}$:	429
Programs:	Bruker[1], SHELX[2,3], Olex2[4]

1 Source of material

Praziquantel and hesperitin purchased from Beijing Mairuida Technology Co., Ltd. were used without further purification. Ethyl acetate was of analytical grade. A mixture of praziquantel (185 mg) and hesperitin (180 mg) in a 1:1 molar ratio, was totally dissolved in 3 mL of ethyl acetate at 313 K. Then the solution was filtered and placed under room temperature. Light yellow, block crystals were obtained after 24 h.

***Corresponding author: Guoshun Zhang**, Department of Pharmacy, Shanxi Medical University, Taiyuan, Shanxi 030001, China, E-mail: zhangguoshunshun@126.com. https://orcid.org/0000-0001-8394-2594

Wei Han, Mei Li and Xiang Geng, Department of Pharmacy, Shanxi Health Vocational College, Jinzhong, Shanxi 030619, China. https://orcid.org/0009-0000-6168-3173 (W. Han)

Table 2: Fractional atomic coordinates and isotropic or equivalent isotropic displacement parameters (Å^2).

Atom	*x*	*y*	*z*	U_{iso}*/U_{eq}
O1	0.13889 (11)	−0.0006 (3)	0.37135 (8)	0.0261 (3)
O2	0.23038 (12)	0.8012 (3)	0.21087 (8)	0.0321 (4)
N1	0.15821 (12)	0.3186 (3)	0.30809 (9)	0.0234 (4)
N2	0.13008 (12)	0.5148 (3)	0.16787 (9)	0.0219 (3)
C1	0.32172 (15)	0.0178 (4)	0.46318 (12)	0.0252 (4)
H1A	0.2739	−0.0593	0.4877	0.030*
H1B	0.3409	−0.0879	0.4268	0.030*
C2	0.41097 (16)	0.0830 (4)	0.52137 (13)	0.0291 (5)
H2A	0.4378	−0.0536	0.5490	0.035*
H2B	0.4613	0.1446	0.4960	0.035*
C3	0.38729 (18)	0.2572 (4)	0.57615 (12)	0.0333 (5)
H3A	0.4479	0.3046	0.6099	0.040*
H3B	0.3441	0.1888	0.6067	0.040*
C4	0.33760 (16)	0.4636 (4)	0.53541 (12)	0.0281 (5)
H4A	0.3190	0.5693	0.5720	0.034*
H4B	0.3837	0.5423	0.5097	0.034*
C5	0.24757 (15)	0.3973 (4)	0.47884 (11)	0.0247 (4)
H5A	0.2180	0.5333	0.4523	0.030*
H5B	0.1993	0.3279	0.5046	0.030*
C6	0.27546 (14)	0.2286 (4)	0.42268 (11)	0.0213 (4)
H6	0.3241	0.3018	0.3972	0.026*
C7	0.18620 (15)	0.1712 (4)	0.36477 (11)	0.0217 (4)
C8	0.20665 (16)	0.5338 (4)	0.30061 (11)	0.0252 (4)
H8A	0.2774	0.5138	0.3180	0.030*
H8B	0.1843	0.6463	0.3334	0.030*
C9	0.18845 (15)	0.6246 (4)	0.22266 (11)	0.0232 (4)
C10	0.06933 (14)	0.3220 (3)	0.17849 (11)	0.0211 (4)
H10	0.0988	0.1812	0.1627	0.025*
C11	0.06242 (14)	0.3017 (4)	0.26020 (10)	0.0219 (4)
H11A	0.0201	0.4229	0.2730	0.026*
H11B	0.0327	0.1550	0.2686	0.026*
C12	0.11823 (16)	0.5965 (4)	0.09152 (11)	0.0263 (4)
H12A	0.1262	0.4705	0.0578	0.032*
H12B	0.1680	0.7122	0.0881	0.032*
C13	0.01750 (16)	0.6973 (4)	0.06920 (12)	0.0283 (5)
H13A	0.0137	0.8383	0.0974	0.034*
H13B	0.0047	0.7350	0.0156	0.034*
C14	−0.05829 (15)	0.5330 (4)	0.08463 (11)	0.0238 (4)
C15	−0.03298 (15)	0.3503 (4)	0.13203 (11)	0.0221 (4)
C16	−0.10368 (16)	0.1899 (4)	0.13930 (12)	0.0279 (5)
H16	−0.0863	0.0619	0.1702	0.033*
C17	−0.19877 (16)	0.2160 (5)	0.10180 (12)	0.0312 (5)
H17	−0.2459	0.1053	0.1068	0.037*
C18	−0.22538 (16)	0.4026 (5)	0.05699 (12)	0.0312 (5)
H18	−0.2909	0.4227	0.0323	0.037*
C19	−0.15510 (15)	0.5600 (4)	0.04857 (12)	0.0271 (4)
H19	−0.1730	0.6880	0.0178	0.033*
O3	−0.66848 (12)	0.3875 (3)	0.04549 (9)	0.0370 (4)
H3	−0.638 (3)	0.498 (8)	0.027 (2)	0.075 (12)*
O4	−0.63103 (12)	0.0534 (3)	0.28502 (8)	0.0327 (4)
H4	−0.678 (2)	−0.043 (6)	0.2626 (17)	0.047 (9)*
O5	−0.55064 (13)	0.7119 (3)	0.03018 (9)	0.0372 (4)
O6	−0.41614 (12)	0.6235 (3)	0.24739 (8)	0.0335 (4)
O7	−0.02989 (13)	0.7807 (3)	0.32084 (10)	0.0384 (4)
H7	0.012 (2)	0.880 (6)	0.3471 (18)	0.052 (9)*
O8	−0.05877 (11)	1.1658 (3)	0.38921 (9)	0.0309 (4)
C20	−0.62116 (15)	0.3730 (4)	0.11661 (12)	0.0279 (5)
C21	−0.65235 (15)	0.2149 (4)	0.16256 (12)	0.0267 (4)
H21	−0.7048	0.1166	0.1437	0.032*
C22	−0.60531 (16)	0.2030 (4)	0.23708 (12)	0.0278 (5)
C23	−0.52780 (17)	0.3465 (4)	0.26551 (12)	0.0315 (5)
H23	−0.4978	0.3405	0.3166	0.038*
C24	−0.49546 (15)	0.4968 (4)	0.21837 (12)	0.0275 (5)
C25	−0.54131 (15)	0.5164 (4)	0.14313 (12)	0.0258 (4)
C26	−0.51026 (16)	0.6839 (4)	0.09559 (12)	0.0290 (5)
C27	−0.42544 (19)	0.8271 (5)	0.13125 (13)	0.0387 (6)
H27A[a]	−0.3866	0.8671	0.0936	0.046*
H27B[a]	−0.4497	0.9687	0.1496	0.046*
H27C[b]	−0.3675	0.7734	0.1132	0.046*
H27D[b]	−0.4382	0.9835	0.1130	0.046*
C28A[b]	−0.4008 (8)	0.8346 (17)	0.2136 (6)	0.029 (3)
H28A[b]	−0.4352	0.9604	0.2338	0.034*
C28B[a]	−0.3630 (2)	0.7096 (6)	0.19365 (15)	0.0282 (9)
H28B[a]	−0.3313	0.5797	0.1731	0.034*
C29	−0.2835 (2)	0.8542 (6)	0.24098 (15)	0.0472 (7)
C30	−0.1926 (2)	0.7651 (5)	0.25825 (14)	0.0430 (7)
H30	−0.1791	0.6252	0.2371	0.052*
C31	−0.11928 (18)	0.8773 (4)	0.30659 (13)	0.0326 (5)
C32	−0.13671 (16)	1.0824 (4)	0.33967 (12)	0.0300 (5)
C33	−0.22727 (18)	1.1792 (5)	0.31943 (15)	0.0419 (6)
H33	−0.2403	1.3228	0.3383	0.050*
C34	−0.30081 (18)	1.0609 (6)	0.26990 (15)	0.0486 (7)
H34	−0.3636	1.1261	0.2564	0.058*
C35	−0.0759 (2)	1.3506 (5)	0.43448 (14)	0.0397 (6)
H35A	−0.0945	1.4835	0.4032	0.060*
H35B	−0.0166	1.3834	0.4710	0.060*
H35C	−0.1283	1.3120	0.4605	0.060*

[a]Occupancy: 0.780 (8), [b]occupancy: 0.220 (8).

2 Experimental details

H atoms bonded to N or O were determined by the experimental electron density map. All other H atoms were located in geometrically calculated positions and refined using a riding model.

3 Comment

Schistosomiasis is a widely prevalent and harmful parasitic disease, with over 230 million people infected worldwide, of which 5 %–10 % of infected individuals will suffer from liver fibrosis.[5] However, liver fibrosis could further develop into cirrhosis, and even liver cancer. Thus, preventing liver fibrosis is of great significance during the treatment of schistosomiasis.

Praziquantel (PZQ) as a derivative of pyrazine isoquinoline, is a potent and preferred drug for the treatment of schistosomiasis with high efficiency and low toxicity.[6] In recent years, it has been also found that PZQ has anti-inflammatory and anti-fibrotic effects in the liver.[7] Hesperetin (HESP) extracted from citrus fruits, is a dihydroflavonoid compound with the pharmacological activities such as antioxidant, anti-inflammatory, anti-apoptotic and anti-tumor[8,9] etc. An increasing number of studies have been reported that HESP also has markedly protective effects against cardiac fibrosis, liver fibrosis and pulmonary fibrosis.[10–12] Therefore, the combination of the above two components may prevent liver fibrosis while treating schistosomiasis.

Cocrystals consist of active pharmaceutical ingredients (APIs) and one or more other cocrystal formers (CCFs) at a definite stoichiometric proportion in the same crystal lattice through noncovalent interactions.[13] Cocrystal technology, as an effective strategy for ameliorating the physico-chemical properties of active pharmaceutical ingredients (API), such as hygroscopicity, dissolution rate, solubility, stability and bioavailability has attracted increasing attention.[14,15] Moreover, the cocrystal technology involving in more than two components, could achieve the combined application of two drugs.[16] Thus, in this study, we aim to synthetize the cocrystal of PZQ and HESP for simultaneously treating schistosomiasis and preventing liver fibrosis.

Here, we successfully prepared the cocrystal of PZQ–HESP through cooling recrystallization method. The complete set of X-ray diffraction data for the title compound was deposited to the Cambridge Crystallographic Data Center (CCDC entry no. 2377413). PZQ–HESP crystallizes in a monoclinic space group $P2_1$ with one PZQ molecule and one HESP molecule in the asymmetric unit. The C27–C28 in PZQ–HESP is disordered and split into two positions. The hydrogen atom of the phenolic hydroxyl group from HESP was not transferred to PZQ, indicating that the obtained product is cocrystal rather than salt.

Intramolecular hydrogen bond with O3–H···O5 in PZQ–HESP was generated to form a five-membered ring-like structure. PZQ molecule and HESP molecule were connected alternately together via intermolecular hydrogen bond with O4–H···O2 and O7–H···O1. The torsion angles for C10–N2–C12–C13 with 67.504°, N1–C8–C9–N2 with 2.016° and N1–C7–C6–C1 with –157.037° in PZQ–HESP respectively, were different from those in PZQ.[16] In addition, the calculated angle between the mean planes of the amide functions with N1–C7–O1 and N2–C9–O2 in PZQ–HESP was 24.494°. Those demonstrated that the conformation of the PZQ molecule had undergone a certain change after the formation of a PZQ cocrystal.

The density of the reported PZQ with 1.250 g/cm^3 was remarkably lower than the obtained cocrystal of PZQ–HESP with 1.362 g/cm^3, indicating that the tighter packing between molecules in PZQ–HESP was one of the main reasons for cocrystal formation.[16] In addition, the traditional strong hydrogen bonding with O–H···O in PZQ–HESP replaces the weak hydrogen bonding with C–H···O in PZQ.[14] This signifies that the stronger intermolecular force in PZQ–HESP relative to that in PZQ, is also one of the main reasons for the formation of cocrystal.

The Hirshfeld surface analysis for PZQ–HESP was performed using Crystal Explorer 17.5[17] and its fingerprint plots were explored to obtain quantitatively various intermolecular interactions. It is obvious that the H···H interactions with 51.4 %, O···H interactions with 25.7 % and C···H interactions with 18.7 % contributed significantly to the Hirshfeld surfaces.

Author contributions: All the authors have accepted responsibility for the entire content of this submitted manuscript and approved submission.
Research funding: The work was sponsored by the Scientific Research Project of Shanxi Health Committee (2019093).
Conflict of interest statement: The authors declare no conflicts of interest regarding this article.

References

1. Bruker. SAINT, APEX2 and SADABS; Bruker AXS Inc.: Madison, WI, USA, 2012.
2. Sheldrick, G. M. SHELXTL – Integrated Space-Group and Crystal-Structure Determination. *Acta Crystallogr.* **2015**, *A71*, 3–8.
3. Sheldrick, G. M. Crystal Structure Refinement with SHELXL. *Acta Crystallogr.* **2015**, *C71*, 3–8.
4. Dolomanov, O. V.; Bourhis, L. J.; Gildea, R. J.; Howard, J. A. K.; Puschmann, H. OLEX2: A Complete Structure Solution, Refinement and Analysis Program. *J. Appl. Crystallogr.* **2009**, *42*, 339–341.
5. Colley, D. G.; Bustinduy, A. L.; Secor, W. E.; King, C. H. Human Schistosomiasis. *Lancet* **2014**, *383*, 2253–2264.
6. de Moraes, M. G. F.; Barreto, A. G.; Secchi, A. R.; de Souza, M. B.; Lage, P. L. d. C.; Myerson, A. S. Polymorphism of Praziquantel: Role of Cooling Crystallization in Access to Solid Forms and Discovery of New Polymorphs. *Cryst. Growth Des.* **2023**, *23*, 1247–1258.
7. Liang, Y. J.; Luo, J.; Yuan, Q.; Zheng, D.; Liu, Y. P.; Shi, L.; Zhou, Y.; Chen, A. L.; Ren, Y. Y.; Sun, K. Y.; Sun, Y.; Wang, Y.; Zhang, Z. S. New Insight into the Antifibrotic Effects of Praziquantel on Mice in Infection with Schistosoma Japonicum. *PLoS One* **2011**, *6*, e20247.
8. Elango, R.; Athinarayanan, J.; Subbarayan, V. P.; Lei, D. K. Y.; Alshatwi, A. A. Hesperetin Induces an Apoptosis-Triggered Extrinsic Pathway and a p53-Independent Pathway in Human Lung Cancer H522 Cells. *J. Asian Nat. Prod. Res.* **2018**, *20*, 559–569.
9. Kim, D. S.; Lim, S. B. Semi-Continuous Subcritical Water Extraction of Flavonoids from Citrus Unshiu Peel: Their Antioxidant and Enzyme Inhibitory Activities. *Antioxidants* **2020**, *9*, 360.

10. Kong, R.; Wang, N.; Luo, H.; Lu, J. Hesperetin Mitigates Bile Duct Ligation-Induced Liver Fibrosis by Inhibiting Extracellular Matrix and Cell Apoptosis via the TGF-Beta1/Smad Pathway. *Curr. Mol. Med.* **2018**, *18*, 15–24.
11. Wang, B.; Li, L.; Jin, P.; Li, M.; Li, J. Hesperetin Protects Against Inflammatory Response and Cardiac Fibrosis in Postmyocardial Infarction Mice by Inhibiting Nuclear Factor κB Signaling Pathway. *Exp. Ther. Med.* **2017**, *14*, 2255–2260.
12. Li, S.; Shao, L.; Fang, J.; Zhang, J.; Chen, Y.; Yeo, A. J.; Lavin, M. F.; Yu, G.; Shao, H. Hesperetin Attenuates Silica-Induced Lung Injury by Reducing Oxidative Damage and Inflammatory Response. *Exp. Ther. Med.* **2021**, *21*, 297.
13. Wang, F. Y.; Zhang, Q.; Zhang, Z.; Gong, X.; Wang, J. R.; Mei, X. Solid-State Characterization and Solubility Enhancement of Apremilast Drug-Drug Cocrystals. *CrystEngComm* **2018**, *20*, 5945–5948.
14. Roca-Paixão, L.; Correia, N. T.; Danède, F.; Guerain, M.; Affouard, F. Carbamazepine/Tartaric Acid Cocrystalline Forms: When Stoichiometry and Synthesis Method Matter. *Cryst. Growth Des.* **2022**, *23*, 1355–1369.
15. Li, J. M.; Dai, X. L.; Li, G. J.; Lu, T. B.; Chen, J. M. Constructing Anti-Glioma Drug Combination with Optimized Properties Through Cocrystallization. *Cryst. Growth Des.* **2018**, *18*, 4270–4274.
16. Espinosa-Lara, J. C.; Guzman-Villanueva, D.; Arenas-García, J. I.; Herrera-Ruiz, D.; Rivera-Islas, J.; Román-Bravo, P.; Morales-Rojas, H.; Höpfl, H. Cocrystals of Active Pharmaceutical Ingredients-Praziquantel in Combination with Oxalic, Malonic, Succinic, Maleic, Fumaric, Glutaric, Adipic, and Pimelic Acids. *Cryst. Growth Des.* **2012**, *13*, 169–185.
17. Spackman, P. R.; Turner, M. J.; McKinnon, J. J.; Wolff, S. K.; Grimwood, D. J.; Jayatilaka, D.; Spackman, M. A. CrystalExplorer: A Program for Hirshfeld Surface Analysis, Visualization and Quantitative Analysis of Molecular Crystals. *J. Appl. Crystallogr.* **2021**, *54*, 1006–1011.